Hopping-Induced Ground-State Magnetism in 6*H* Perovskite Iridates

A. Nag,[1,*] S. Bhowal,[2,†] M. Moretti Sala,[3,4] A. Efimenko,[3] I. Dasgupta,[2] and Sugata Ray[1,‡]
[1]School of Materials Science, Indian Association for the Cultivation of Science, Jadavpur, Kolkata 700032, India
[2]School of Physical Sciences, Indian Association for the Cultivation of Science, Jadavpur, Kolkata 700032, India
[3]ESRF-The European Synchrotron, 71 Avenue des Martyrs, 38000 Grenoble, France
[4]Dipartimento di Fisica, Politecnico di Milano, Piazza Leonardo da Vinci 32, I-20133 Milano, Italy

(Received 12 January 2019; revised manuscript received 5 April 2019; published 1 July 2019)

Investigation of elementary excitations has advanced our understanding of many-body physics governing most physical properties of matter. Recently spin-orbit excitons have drawn much attention, whose condensates near phase transitions exhibit Higgs mode oscillations, a long-sought-after physical phenomenon [A. Jain, *et al.*, Nat. Phys. **13**, 633 (2017)]. These critical transition points, resulting from competing spin-orbit coupling (SOC), local crystalline symmetry, and exchange interactions, are not obvious in iridium-based materials, where SOC prevails in general. Here, we present results of resonant inelastic x-ray scattering on a spin-orbital liquid $Ba_3ZnIr_2O_9$ and three other 6*H*-hexagonal perovskite iridates that show magnetism, contrary to the nonmagnetic singlet ground state expected due to strong SOC. Our results show that substantial hopping between closely placed Ir^{5+} ions within Ir_2O_9 dimers in these 6*H* iridates modifies spin-orbit coupled states and reduces spin-orbit excitation energies. Here, we are forced to use at least a two-site model to match the excitation spectrum going in-line with the strong intradimer hopping. Apart from SOC, low-energy physics of iridates is thus critically dependent on hopping and may not be ignored even for systems having moderate hopping, where the excitation spectra can be explained using an atomic model. SOC, which is generally found to be 0.4–0.5 eV in iridates, is scaled in effect down to ~0.26 eV for the 6*H* systems, sustaining the hope of achieving quantum criticality by tuning Ir-Ir separation.

DOI: 10.1103/PhysRevLett.123.017201

Competition between lattice, spin, and orbital degrees of freedom is often responsible for remarkable properties in condensed-matter systems [1]. While atomic spin-orbit coupling is quenched in light transition metal oxides, it starts influencing physical properties in 4*d* or 5*d* systems [2–4]. In these materials, spin-orbit coupling (SOC or λ) manifests itself by splitting wide *d* bands and effectively enhancing electronic correlations resulting in Mott-insulating states akin to 3*d* oxides [5,6]. A magnetic condensation of excitations across spin-orbit-coupled states (SOC states) in some of these Mott insulators [d^4 systems, whose ground states are expected be nonmagnetic SOC $J = 0$ (J_0) singlets, with S, L nominally equal to one] was predicted by Khaliullin [7], of which Ca_2RuO_4 has been an exemplary case [8]. With the free-ion SOC itself being small in the $4d^4$ oxides like Ca_2RuO_4 [8,9], SOC states are readily perturbed by noncubic crystal fields (Δ_{CF}^{NC}) around the $4d^4$ ions, allowing access to the magnetic $J = 1$ (J_1) triplet states. In Ir^{5+} systems, however, the prediction seems to have stayed experimentally unclear and debated on account of stronger SOC that raises the excitation energies (0.37 eV) compared to the intersite exchange interactions [2,4]. In addition, it has been shown recently that even a large Δ_{CF}^{NC} (0.325 eV), fails to compete with strong SOC to close the spin-orbit excitation gap comprehensively [3].

Interestingly, in these systems either the Ir^{5+} ions are far apart, intervened by closed shell ions (Fig. 1) [2,4], or are within corner or edge-shared octahedral geometries [10]. In contrast, significant magnetic responses are obtained from 6*H*-hexagonal perovskite iridates $Ba_3MIr_2O_9$, (M = Mg, Zn, Ca, and Sr), where the Ir^{5+} ions form face-sharing octahedral dimeric units [Fig. 1(a)] [11–13]. Since each Ir^{5+} ion in such a situation "sees" another Ir^{5+} ion as its nearest neighbor, hopping between them via O^{2-} ions becomes important [13,14]. In addition to these three Ir-O-Ir superexchange pathways, the small intradimer Ir-Ir distances (about 2.7 Å) [13] provide for direct exchanges between the Ir^{5+}'s. For example, bandwidths ($W = 2zt_{eff}$) obtained from density functional theory (DFT) without the influence of SOC give the effective hopping t_{eff} to be 0.06 eV in double perovskite (DP) Ba_2YIrO_6, while in 6*H* $Ba_3ZnIr_2O_9$ it is around 0.31 eV (see Supplemental Material [15]).

Resonant inelastic x-ray scattering (RIXS), a second order "photon-in, photon-out" spectroscopic technique, has emerged to be particularly suited to study the hierarchy of these SOC states in iridates [16–19]. The process is sensitive to the changes in energy, momentum, and polarization of inelastically scattered x-ray photons representing elementary excitations in a material. With the development of high-resolution spectrometers [20], it is now possible to

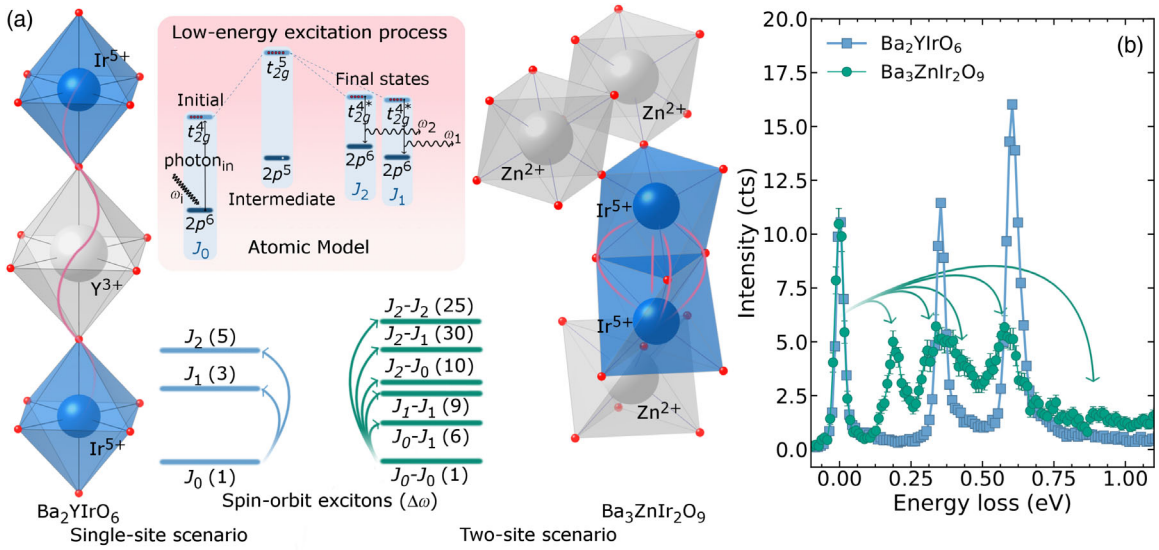

FIG. 1. Enhanced intersite hopping rendering possibility of magnetic condensation in $6H$ iridates. (Inset) Spin-orbit excitonic process occurring in RIXS (represented by curved arrows in main panel) shown schematically. SOC states higher in energy are not shown for clarity, as transitions to them have low spectral intensities. See text for details. (a) As one goes from double perovskites like Ba_2YIrO_6, where the Ir^{5+} ions are far apart, to $6H$-hexagonal perovskites like $Ba_3ZnIr_2O_9$, where the Ir^{5+} ions form a dimer, inclusion of effective intersite hopping creates two-site SOC states (J_0-J_0, J_0-J_1, etc.). (b) Comparison of the low-energy RIXS spectra from the SOC states in Ba_2YIrO_6 to $Ba_3ZnIr_2O_9$ showing energy-loss peaks corresponding to excitations to the SOC states. The presence of additional inelastic peaks and spectral-weight transfer to lower energies make it impossible to describe $Ba_3ZnIr_2O_9$ using the atomic model.

resolve low-energy excitations to such SOC states in a RIXS experiment [2,21]. The low-energy spin-orbit excitonic process for an atomic scenario is depicted in the inset of Fig. 1(a) and explained below. Strictly within an atomic model with strong octahedral crystal field and SOC, $5d^4$ electrons in t_{2g} orbitals have their spins $S = 1$ coupled to orbital angular momenta $L = 1$, forming nominally nonmagnetic SOC states of $J = 0$ (J_0). The incoming photons with energy ω_i excite the system from $|i\rangle = |2p^6 t_{2g}^4\rangle$ initial state to an intermediate $|n\rangle = |2p^5 t_{2g}^5\rangle$ state with core holes. This excited state then decays into a final state $|f\rangle = |2p^6 t_{2g}^{4*}\rangle$, different from the initial state in terms of the arrangement of the SOC electrons ($(6!/4!2!) - 1$ possibilities), and in the process emits photons of energy ω_1,ω_2 and so on. The energy losses $\Delta\omega = \omega_i - \omega_1, \omega_2$ then correspond to the energy costs for the different arrangements of the electrons within the SOC t_{2g} orbitals. Even though RIXS has already been employed to study spin-orbit excitations in DP Ir^{5+} systems, marginal intersite hopping has had an undetectable effect on the RIXS spectra, which could be interpreted by a bare atomic model [2,4,15,21]. In contrast, we here show using RIXS that enhancement in intersite hopping due to close placement of Ir^{5+} ions drives the $6H$ iridates [$Ba_3MIr_2O_9$ (M = Mg, Zn, Ca, and Sr)] into a regime where the effective SOC strength is weakened and the ground state deviates from nonmagnetic singlets (Fig. 1). This is the first observation of spin-orbit excitons having such low energies in Ir^{5+} systems [2,4]. Since an atomic model fails [15], particularly, to explain a low-energy peak around 0.2 eV and a two-peak feature around 0.4 eV as shown in Fig. 1(b), we implement exact diagonalization of a minimal two-site model including the influences of physical parameters [λ, $\Delta_{\mathrm{CF}}^{\mathrm{NC}}$, Hunds coupling J_H, and intradimer hopping (t_{dim})] to map the low-energy excitations in RIXS spectra. We find that the observed features are characteristic of a two-site model with a finite intersite hopping (see Fig. 1). This is not surprising given the fact that the Ir ions in these $6H$ iridates interact strongly with their nearest neighbors, forming Ir-Ir dimers [11,13], in comparison to DP iridates, where the Ir ions have little interaction. Strangely, however, we find that λ, usually considered to be 0.4–0.5 eV for iridates, is scaled down effectively to ~0.26 eV in the presence of strong t_{dim}. Moderate hopping in other systems like Ba_2YIrO_6 may similarly be suspected to rescale the atomic λ, even though imperceptible in RIXS [4].

In order to characterize the spin-orbit excitons in the presence of intradimer hopping (beyond the capacity of single-particle theories), we have employed many-body multiplet formalism incorporated within the following two-site model Hamiltonian for the Ir-t_{2g} orbitals [22,23]:

$$H = \sum_{i=1,2} (H_i^{\Delta_{\mathrm{CF}}^{\mathrm{NC}}} + H_i^{\mathrm{int}} + H_i^{\mathrm{SO}}) + H^t, \qquad (1)$$

where $H_i^{\Delta_{\mathrm{CF}}^{\mathrm{NC}}}$, H_i^{int}, and H_i^{SO} are the respective Hamiltonians representing the noncubic crystal field, Coulomb interactions, and SOC for the ith site. H_i^{int}, known as the

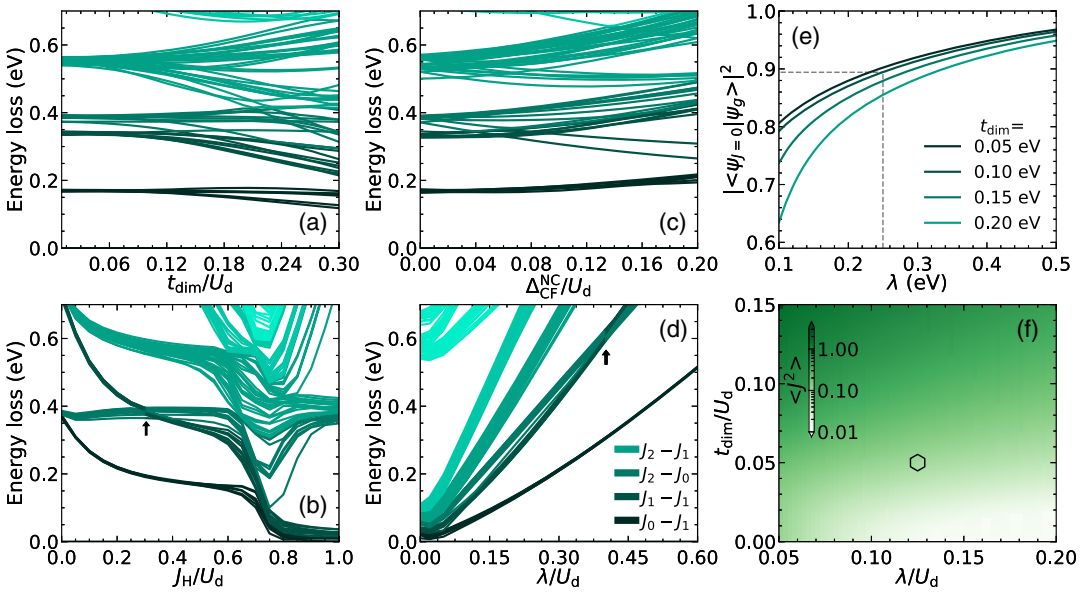

FIG. 2. (a)–(d) Effects of varying physical parameters t_{dim}/U_d, J_H/U_d, $\Delta_{\mathrm{CF}}^{\mathrm{NC}}/U_d$, and λ/U_d respectively, on the SOC excitonic gaps, evaluated using the two-site model Hamiltonian given in Eq. (1). Each set of SOC states is named after their parent atomic SOC states and colored with a different shade as labeled in (d). (e) For $\lambda = 0.25$ eV (relevant for the $6H$ iridates), the two-site ground state (ψ_g) deviates from the $J = 0$ state by about 10%. The phase diagram in (f) shows the variation of the $\langle J^2 \rangle$ expectation value in the parameter space of t_{dim}/U_d and λ/U_d. The mark denotes the estimated $J \neq 0$ scenario in the $6H$ iridates. Parameters of the Hamiltonian are (unless its variation has been shown) $t_{\mathrm{dim}} = 0.1$, $\Delta_{\mathrm{CF}}^{\mathrm{NC}} = 0.02$, $J_H = 0.5$, $\lambda = 0.25$, and $U_d = 2.0$ eV.

Kanamori Hamiltonian, includes intra- (U_d) and interorbital (U'_d) Coulomb interactions alongside Hund's coupling (J_H) and are related by $U_d = U'_d + 2J_H$ (see Supplemental Material for detailed expressions) [15]. In addition to these on site terms, we introduce H^t to account for intersite hopping $t_{ij}^{l\sigma,m\sigma'}$ between the three t_{2g} orbitals at the two Ir^{5+} sites i and j. While within the atomic model [15], SOC gives rise to multiplet states J_0, J_1, J_2, … [see Fig. 1(a)], in the presence of strong t_{dim} these SOC states are influenced by neighboring atomic multiplet states, forming two-site SOC states [shown schematically in Fig. 1(a)]. The spin-orbit exciton energies can be obtained from the difference in energy eigenvalues calculated using exact diagonalization of the two-site model. Because of the inclusion of intersite hopping in the two-site model, new sets of SOC states appear out of the interaction between the atomic SOC states at the two sites: J_0-J_0 (1), J_0-J_1 (6), J_1-J_1 (9), J_0-J_2 (10), J_1-J_2 (30), J_2-J_2 (25), etc. The new sets of two-site SOC states are denoted according to their parent atomic SOC states (J_0-J_0, J_0-J_1, etc.) and the numbers within the parentheses indicate the number of SOC states having the same origin. Excitations from the J_0-J_0 SOC states to the sets originating from the interaction between atomic SOC states J_1-J_1 or J_0-J_2 form the inelastic features in the RIXS spectra. The fact that strong intradimer hopping plays a key role in modifying the low-energy SOC excitation spectrum is directly verified from the experimental results [Fig. 1(b)].

In our calculation, we have assumed the hopping to be diagonal in the spin space, i.e., $t_{\mathrm{dim}} = t_{ij}^{l\sigma,m\sigma}$. Also we have supposed that the hopping parameters are diagonal and equal in the orbital space to illustrate the effect of different parameters on the energies of the spin-orbit excitons (Fig. 2). A trigonal crystal field is also assumed in this case. However, more realistic hopping and noncubic matrices guided by the first principles calculations are considered to fit the RIXS spectra of the $6H$ iridates. It is important to note that the noncubic crystal field and the hopping terms take care of the nonlocal effects within the solid. Such a simple t_{2g}-only two-site model captures the essential features of these $6H$ iridates owing to the dimeric interaction and large t_{2g}-e_g splitting [allowing us to neglect the e_g orbitals (see Supplemental Material Fig. 2)] [15]. Taking into account the $\Delta_{\mathrm{CF}}^{\mathrm{NC}}$ and t_{dim} ($= t_{ij}^{l\sigma,m\sigma'}$), which are both set up in part by O^{2-} ions, also indirectly includes their effects in the model. Figure 2 shows the influence of each of these physical parameters on the excitonic gaps within the two-site model calculation. In contrast to the atomic states, spin-orbit excitation energies obtained from the two-site model also depend on Coulomb repulsion U_d since the superexchange energy varies as $\sim t_{\mathrm{dim}}^2/U_d$ in the latter case. It is clear from Figs. 2(a)–2(d) that $\Delta_{\mathrm{CF}}^{\mathrm{NC}}$ and t_{dim} control the spread of each set of states, while their mean energies are primarily dictated by J_H and λ. An interesting feature in the spin-orbit exciton energy spectrum is the crossover between J_0-J_2 and J_1-J_1 states as we go from $J_H \ll \lambda$ to the $J_H \gg \lambda$ limit [15]. Even though this two-site model is a simplistic representation of processes in a real solid, it illustrates how hopping affects

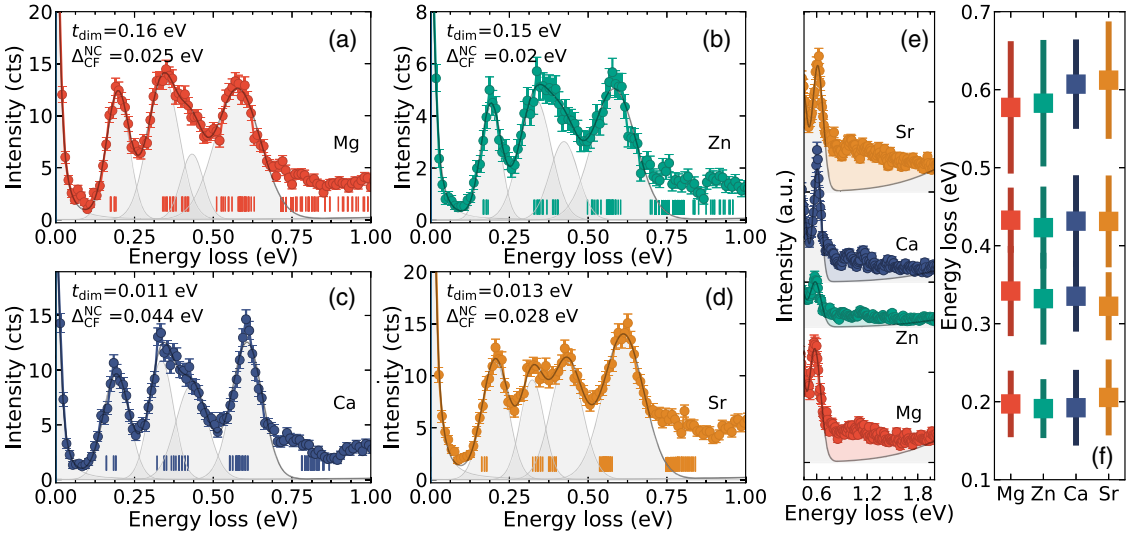

FIG. 3. Low-energy RIXS spectra from the 6*H* iridates and energy losses corresponding to the two-site SOC states. Each spectrum is decomposed into four sets of spin-orbit excitations by fitting Gaussian line shapes (shaded gray) (a)–(d). Vertical bars represent energies of two-site SOC states evaluated using $J_H = 0.5$ and $\lambda = 0.25$ eV in Eq. (1) and parameters given in each panel. (e) The spectra are shifted vertically to show continua of low-intensity excitations above the well-defined peaks (shaded regions between the spectra and Gaussian tails from e_g peaks). Fitted peak positions (squares) and peak FWHM (length of the vertical lines through the squares) for the four 6*H* iridates shown in (a)–(d) are presented in (f).

low-energy RIXS spectra of the 6*H* perovskite iridates as shown later. Most important, as seen from Fig. 2(e) is that, for $\lambda = 0.25$ eV (relevant for the 6*H* iridates), the two-site ground state deviates from the $J = 0$ state by about 10% and, as a consequence, the expectation value $\langle J^2 \rangle$ of the ground state attains a nonzero value and hence small moments.

High-resolution (0.029 eV at Ir-L_3 edge) RIXS spectra of the 6*H* iridates ($Ba_3MIr_2O_9$, M = Mg, Zn, Ca, and Sr), collected at 20 K at the ID20 beam line of ESRF, The European Synchrotron at 20 K [20], are shown in Figs. 3(a)–3(d), all of which show similar low-energy inelastic features, unlike the RIXS from DPs like Ba_2YIrO_6 [see Fig. 1(b)], exhibiting the strong influence of intradimer hopping in these systems. The inelastic features of each spectrum are fitted with four Gaussian line shapes representing excitations from the J_0-J_0 state to higher lying two-site SOC states (see Supplemental Material for details) [15]. Since excitations to the set of SOC states J_1-J_1 and J_2-J_0 are not clearly resolved [strongest splitting is seen for $Ba_3SrIr_2O_9$, Fig. 3(d)], the fits to these two sets of peaks are done by limiting their Gaussian variances to 0.05 eV. A Gaussian tail from the high-energy $t_{2g} - e_g$ excitation peak is also included in the fitting, although its effect on the four SOC peaks is minimal [Fig. 3(e)]. Although, excitations within the higher-energy states cannot be ruled out given their strong intermixing, these excitations would have comparatively weak intensities and are not resolved in the present experiments. A broad continuum of excitations can be seen [Fig. 3(e)] above 0.7 eV in all the systems that may be related to low-intensity transitions to J_2-J_2 states besides multiparticle excitations [18,19]. We note that the spectral weights of the J_2-J_2 excitation features (~0.75 eV) are substantially suppressed in spite of large number of states for all of the four systems, again showing significant hopping-induced deviation of these states anticipated from the pure atomic descriptions (see Supplemental Material Fig. 5) [15].

The peak positions and their widths extracted from the fitting of the energy-loss features are shown in Fig. 3(f). The slight variation in the peak positions and widths are related to the details of the local geometry of these four iridates. This becomes evident when we try to place the difference in eigenvalues obtained from the exact diagonalization of the two-site model Hamiltonian given in Eq. (1) with different parameters, within the FWHM of these peaks (Supplemental Material Fig. 4) [15].

For the two smaller cations Mg^{2+} (0.72 Å) and Zn^{2+} (0.74 Å), the compounds $Ba_3MgIr_2O_9$ and $Ba_3ZnIr_2O_9$ stabilize in a $P6_3/mmc$ space group, while Ca^{2+} (1.00 Å) and Sr^{2+} (1.18 Å) allow formation of $Ba_3CaIr_2O_9$ and $Ba_3SrIr_2O_9$ only within a lower symmetry space group $C2/c$ [11–13,15,24]. Each of these 6*H* iridates therefore possesses a slightly modified IrO_6 octahedral environment resulting in different t_{dim} and Δ_{CF}^{NC} values. We find that RIXS spectra for the 6*H* iridates can be fitted over a small range of values for all the parameters (Supplemental Material Table II) [15]. A realistic estimation of hopping and noncubic crystal field energies for the different local geometries of the Ir^{5+} ions in the 6*H* iridates is obtained by extracting the low-energy tight-binding model retaining only Ir-t_{2g} in the basis from the muffin-tin orbital (MTO)-based *N*th order MTO (NMTO) method [25–27]

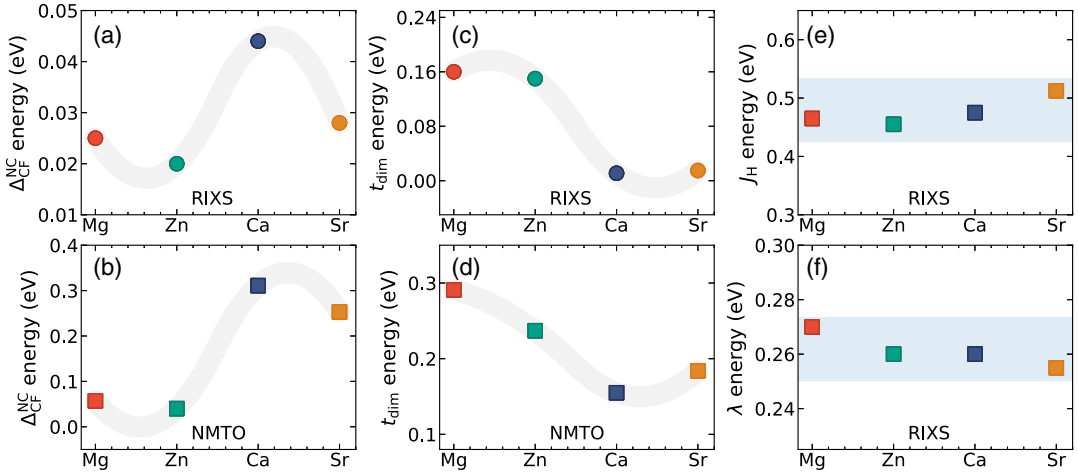

FIG. 4. Comparison of physical parameters obtained from DFT to the ones extracted by fitting RIXS spectra with two-site model Hamiltonian for the 6*H* iridates. Energy-loss values associated with SOC states were calculated using the two-site model Hamiltonian (1) and matched to experimentally obtained inelastic features, by varying Δ_{CF}^{NC}, t_{dim}, J_H, and λ. Maximum components of Δ_{CF}^{NC}, t_{dim} matrices for each system giving best fits to RIXS are shown in (a) and (c), respectively (see text). (b),(d) Corresponding values obtained from DFT calculations using NMTO. The points are connected by shaded splines of degree 2 to emphasize similar variation in values obtained using the two methods. (e),(f) Average values of J_H and λ obtained for the best fits to RIXS spectra in each system.

as implemented in the Stuttgart code. While $P6_3/mmc$ symmetry of $Ba_3MgIr_2O_9$ and $Ba_3ZnIr_2O_9$ leads to trigonal distortion of the IrO_6 octahedra, so that Ir-t_{2g} orbitals split into singly degenerate a_{1g} and e_g^{π} states, monoclinic distortions in $Ba_3CaIr_2O_9$ and $Ba_3SrIr_2O_9$ remove completely the degeneracy of the t_{2g} states and are reflected accordingly in the noncubic crystal field matrices (see Supplemental Material Sec. V) [15]. This results in diagonal hopping matrices for $Ba_3MgIr_2O_9$ and $Ba_3ZnIr_2O_9$, while $Ba_3CaIr_2O_9$ and $Ba_3SrIr_2O_9$ have relatively complicated forms with nonzero off-diagonal elements (see Supplemental Material Sec. VI) [15]. The values obtained from the first principles calculations are taken as initial guesses and are then renormalized to fit the RIXS spectra, while keeping the ratios between different elements of the matrices for hopping and noncubic crystal field fixed to that obtained from DFT. Parameters of the Hamiltonian that give energy-loss values within the FWHM of the Gaussian fits to the RIXS peaks are then extracted as shown in Supplemental Material Figs. 4(a)–4(d) [15]. In our calculations, we keep the value of U_d fixed at 2 eV [2].

The best matched energy-loss values of the two-site SOC states calculated using a set of values for the parameters Δ_{CF}^{NC}, t_{dim}, J_H, and λ for each of the four systems are shown as vertical bars in Figs. 3(a)–3(d). The maximum components of Δ_{CF}^{NC} and t_{dim} matrices used for the fits are then compared to the corresponding values obtained using the NMTO method on these systems in Figs. 4(a)–4(d). We find that the parameters extracted from RIXS are scaled down with respect to the ones obtained from first principles. However, as can be seen from Figs. 4(a)–4(d), the reduction in values is not arbitrary and is qualitatively similar for the four 6*H* iridates. It should be mentioned here that overestimation of parameters from first principles is known and reported for honeycomb iridates with d^5 electronic configuration [28]. Hund's coupling estimated from RIXS (~0.45 eV) is similar for all four [see Fig. 4(e)], comparable to other $5d^5$ systems, but higher than the $5d^4$ DP iridates [2,21]. However, most striking is the substantially suppressed value of SOC (~0.26 eV) compared to any other iridate reported as yet, proving the decisive role of intradimer hopping in these systems. In this context, reduced covalency has recently been ascribed to increased SOC in iridium fluorides [29]. RIXS of these 6*H* iridates provide the first clear experimental evidences of atomic nonmagnetic SOC $J = 0$ state breakdown, in the presence of solid-state effects. The two-site model can also be applied to describe the low-energy physics of other systems where the Ir ions are placed close by in the crystal structure [30–33]. Estimating deviation of the SOC dimerized states from their atomic limits using methods presented in a recent work [33], can provide further insights into these states. The polycrystalline nature of our samples and two-site theoretical modeling forbid estimation of the momentum dependence of the spin-orbit excitons presently and can be a future direction of work. The identification of intersite hopping as a critical parameter that can drastically change the effective strength of SOC, may be utilized to tune magnetism in iridates.

S. R. and I. D. G. thank the Technical Research Center of IACS. S. R. also thanks the Department of Science and Technology (DST) (Project No. WTI/2K15/74), UGC-DAE Consortium for Scientific Research, Mumbai, India (Project No. CRS-M-286) for support, and Jawaharlal

Nehru Centre for Advanced Scientific Research from the DST-Synchrotron-Neutron project, for performing experiments at ESRF (Proposal No. HC-2872). A. N. thanks M. P. M. Dean for useful comments about the result. I. D. G. thanks Science and Engineering Research Board (SERB), India (Project No. EMR/2016/005925) for support.

[*]Present address: Diamond Light Source, Harwell Campus, Didcot OX11 0DE, United Kingdom.
[†]Present address: Department of Physics and Astronomy, University of Missouri, Columbia, Missouri 65211, USA.
[‡]mssr@iacs.res.in

[1] J. G. Rau, E. K. Lee, and H. Y. Kee, Annu. Rev. Condens. Matter Phys. **7**, 195 (2016).
[2] M. Kusch *et al.*, Phys. Rev. B **97**, 064421 (2018).
[3] S. Agrestini *et al.*, Phys. Rev. B **97**, 214436 (2018).
[4] A. Nag *et al.*, Phys. Rev. B **98**, 014431 (2018).
[5] B. J. Kim *et al.*, Phys. Rev. Lett. **101**, 076402 (2008).
[6] M. Imada, A. Fujimori, and Y. Tokura, Rev. Mod. Phys. **70**, 1039 (1998).
[7] G. Khaliullin, Phys. Rev. Lett. **111**, 197201 (2013).
[8] A. Jain *et al.*, Nat. Phys. **13**, 633 (2017).
[9] S.-M. Souliou, J. Chaloupka, G. Khaliullin, G. Ryu, A. Jain, B. J. Kim, M. LeTacon, and B. Keimer, Phys. Rev. Lett. **119**, 067201 (2017).
[10] L. Du, X. Sheng, H. Weng, and X. Dai, Europhys. Lett. **101**, 27003 (2013).
[11] A. Nag *et al.*, Phys. Rev. Lett. **116**, 097205 (2016).
[12] T. Sakamoto, Y. Doi, and Y. Hinatsu, J. Solid State Chem. **179**, 2595 (2006).
[13] A. Nag *et al.*, Phys. Rev. B **97**, 064408 (2018).
[14] K. I. Kugel, D. I. Khomskii, A. O. Sboychakov, and S. V. Streltsov, Phys. Rev. B **91**, 155125 (2015).
[15] See Supplemental Material at http://link.aps.org/supplemental/10.1103/PhysRevLett.123.017201, which includes details of the experiments and theory.
[16] L. J. P. Ament, G. Khaliullin, and J. van den Brink, Phys. Rev. B **84**, 020403(R) (2011).
[17] M. M. Sala, K. Ohgushi, A. Al-Zein, Y. Hirata, G. Monaco, and M. Krisch, Phys. Rev. Lett. **112**, 176402 (2014).
[18] B. J. Kim and G. Khaliullin, Phys. Rev. B **96**, 085108 (2017).
[19] A. Paramekanti, D. J. Singh, B. Yuan, D. Casa, A. Said, Y. J. Kim, and A. D. Christianson, Phys. Rev. B **97**, 235119 (2018).
[20] M. M. Sala *et al.*, J. Synchrotron Radiat. **25**, 580 (2018).
[21] B. Yuan *et al.*, Phys. Rev. B **95**, 235114 (2017).
[22] H. Matsuura and K. Miyake, J. Phys. Soc. Jpn. **82**, 073703 (2013).
[23] S. Bhowal and I. Dasgupta, Phys. Rev. B **97**, 024406 (2018).
[24] R. D. Shannon, Acta Crystallogr., Sect. A **32**, 751 (1976).
[25] O. K. Andersen and T. Saha-Dasgupta, Phys. Rev. B **62**, R16219 (2000).
[26] O. K. Andersen *et al.*, *Electronic Structure and Physical Properties of Solids. The Uses of the LMTO Method*, Springer Lecture Notes in Physics (Springer, Berlin, 2000), p. 3.
[27] O. K. Andersen, T. Saha-Dasgupta, and S. Ezhov, Bull. Mater. Sci. **26**, 19 (2003).
[28] B. H. Kim, T. Shirakawa, and S. Yunoki, Phys. Rev. Lett. **117**, 187201 (2016).
[29] M. Rossi, M. Retegan, C. Giacobbe, R. Fumagalli, A. Efimenko, T. Kulka, K. Wohlfeld, A. I. Gubanov, and M. Moretti Sala, Phys. Rev. B **95**, 235161 (2017).
[30] T. Takayama *et al.*, https://arxiv.org/abs/1808.05494.
[31] S. V. Streltsov, G. Cao, and D. I. Khomskii, Phys. Rev. B **96**, 014434 (2017).
[32] K. Ishii, I. Jarrige, M. Yoshida, K. Ikeuchi, J. Mizuki, K. Ohashi, T. Takayama, J. Matsuno, and H. Takagi, Phys. Rev. B **83**, 115121 (2011).
[33] Y. Wang, R. Wang, J. Kim, M. H. Upton, D. Casa, T. Gog, G. Cao, G. Kotliar, M. P. M. Dean, and X. Liu, Phys. Rev. Lett. **122**, 106401 (2019).